

MINIATURE OPTICAL COHERENCE TOMOGRAPHY PROBE

by

ASIF RIZWAN

Presented to the Faculty of the Graduate School of  
The University of Texas at Arlington in Partial Fulfillment  
of the Requirements  
for the Degree of

MASTER OF SCIENCE IN BIOMEDICAL ENGINEERING

THE UNIVERSITY OF TEXAS AT ARLINGTON

DECEMBER 2006

Copyright © ASIF RIZWAN 2006

All Rights Reserved

## ACKNOWLEDGEMENTS

To Dr. Digant Dave, thank you for giving me the opportunity to work on such an exciting project. Your guidance helped me to obtain a sound understanding of optics. I am grateful, for this appreciation and understanding. To Dr. Shashank Priya and Dr. Liping Tang, thank you for your support, guidance and advice during my research and graduate studies. Thank you.

To my dad and mom, thank you for all your support and inspiration throughout my life. You always encouraged me to follow my dreams. To my sisters Bipasha and Barsha without whose enthusiasms and love none of this would have been possible. My special thanks to Ms. Nidhi and Mr. Manish for their indispensable technical assistance. I take this opportunity to thank all the members of Dr. Dave's group for their cooperation as and when required.

November 15, 2006

## ABSTRACT

### MINIATURE OPTICAL COHERENCE TOMOGRAPHY PROBE

Publication No. \_\_\_\_\_

ASIF RIZWAN, MS

The University of Texas at Arlington, 2006

Supervising Professor: Digant Dave

A piezo based optical scanner for high speed optical coherence tomography (OCT) has been developed. Design of the miniature probe has been optimized to take advantages of the high speed depth scanning that can be achieved with spectral domain OCT (SD-OCT) systems. Three prototype scanning probes were constructed and tested for OCT imaging. Movies and images of tissues are presented which were taken at frame rates ranging from 50~100fps. Data were acquired at 18000 A-lines per second at an effective integration time of 55 $\mu$ s.

## TABLE OF CONTENTS

ACKNOWLEDGEMENTS.....	iii
ABSTRACT .....	iv
LIST OF ILLUSTRATIONS.....	viii
LIST OF TABLES .....	ix
Chapter	
1. INTRODUCTION .....	1
1.1 Background and Significance.....	1
1.1.1 Optical Coherence tomography and Imaging Probe .....	1
1.2 Specific Aim.....	3
1.3 Organization of the thesis .....	3
2. FOURIER DOMAIN OPTICAL COHERENCE TOMOGRAPHY AND PIEZOELECTRIC ACTUATOR.....	5
2.1 Introduction.....	5
2.1.1 Fourier domain Optical Coherence Tomography.....	6
2.1.2 Application of OCT and optical Biopsy.....	9
2.2 Piezoelectric Actuator.....	9
2.2.1 Background information on Piezoelectric.....	9
2.2.2 Background information on Stripe actuator.....	10

2.3 Construction of scanning arm (Probe).....	11
2.3.1 Construction of Probe 1.....	13
2.3.2 Construction of Probe 2 .....	14
2.3.3 Construction of Probe 3.....	15
3. SYSTEM SETUP.....	17
3.1 Setup of Michelson Interferometer .....	17
3.2 Probe setup.....	19
3.2.1 Probe 1 Setup .....	19
3.2.2 Probe 2 Setup .....	20
3.2.3 Probe 3 Setup.....	21
4. CALIBRATION AND CHARACTERIZATION.....	22
4.1 Spectrum Calibration.....	22
4.2 System characterization.....	23
4.2.1 Modulation Index .....	23
4.2.2 Scan length .....	24
4.2.3 Resonant Frequency.....	24
4.2.4 Number of lines per scan.....	24
4.2.5 Resolution.....	25
4.3 Data Acquisition.....	28
5. RESULTS AND ANALYSIS.....	31
5.1 Images Taken By Probe .....	31

6. DISCUSSION AND CONCLUSION.....	33
Appendix	
A. GLOSSARY.....	34
B. SPECIFICATION OF THE PHOTO DETECTOR (PDA520) .....	36
C. BACKGROUND INFORMATION ABOUT STRIPE ACTUATORS .....	38
REFERENCES .....	43
BIOGRAPHICAL INFORMATION .....	48

## LIST OF ILLUSTRATIONS

Figure	Page
1 OCT based on low coherence Michelson interferometry.....	6
2 Schematic figure of the FD-OCT system.....	7
3 Stripe actuator from APC International Ltd.....	10
4 (a) The glass tube housed the glass ferrule where the fiber is placed (b) The actual picture which shows the glass tube, ferrule and the grin lens.....	11
5 (a) Top view of Probe 1 (b) Side view of Probe 1 (c) Actual Picture of the actuator.....	14
6 Actual picture of (a) probe2-a and (b) probe2-b .....	15
7 (a)The schematic diagram of the probe (b) The real figure of the probe.....	16
8 OCT system setup.....	17
9 Ex vivo imaging probe setup.....	19
10 Schematic diagram of Probe2 .....	20
11 Side View of the probe.....	21
12 Illustration of depth of focus and the beam waist.....	26
13 Flowchart for data acquisition using Labview.....	29
14 Flowchart for image processing using Matlab.....	30
15 OCT image of Normal Urinary bladder 1.4mm x 0.72mm. The scale bar represents 120 $\mu$ m.....	32



## LIST OF TABLES

Table		Page
1	Three different types of probes used.....	12
2	Characteristics of three different types of probes used.....	27

## CHAPTER 1

### INTRODUCTION

#### 1.1 Background and Significance

This thesis describes the construction and characterization of piezoelectric probe for Optical coherence tomography imaging. Images were taken using both ex vivo and in vivo OCT probe. The system provides greater flexibilities and portability's compare to the galvo scanner.

##### *1.1.1 Optical Coherence tomography and Imaging Probe*

Optical coherence tomography (OCT) is a noninvasive imaging technique used for cross sectional imaging with micrometer resolution of scattering media such as tissue. [1] Imaging of the internal organ is possible if the actuator of the OCT can be held suitably for in vivo imaging of lips and cheek pouch or if it fits inside the instrumentation channel of the endoscope [2, 3]. The OCT scanners used for lateral scanning provides linear translation of the probing heads instead of the sample. Implementation of the scanner depends strongly on probe size and the space allowed for scanning [4]. Existing scanners can be divided into three types [4]: benchtop hand held and endoscopic. Our miniature probe can be used either as a benchtop or as a handheld scanner. Various scanning components have been tried earlier for benchtop and handheld scanning such as using a MEMS(micro electromechanical system) motor [5],

tube actuator[6], different types of cantilever[4,7,8]. I used rectangular piezoelectric actuators from American Piezoelectric Corporation. The resonant frequency of the actuator has been modified by adding weight. Also width of the actuator has been reduced which does not have any effect on the resonant frequency. The objective of resizing the dimension and reduce the resonant frequency is to make those parameters suitable for in vivo and video rate imaging. Previously different techniques have been demonstrated to do in vivo imaging at 20~40 frame per second [9~13]. I have demonstrated video rate imaging of tissues with our miniature probe at frame rates ranging from 50~100fps. With some rare exceptions, lateral scanning is performed slowly in comparison with in-depth scanning. In conventional time-domain OCT system, the reference mirror is scanned to provide a depth profile within the sample (A-scan). Stacking several A-scans in a direction orthogonal to A-scan gives us a B-Scan image [14, 15, and 16].

Spectral domain or Fourier Domain OCT was developed where the depth information could be obtained from the spectral density of the interferometer with the help of a spectrometer [17, 18, 19, 20, 21]. Spectral domain has the advantages in terms of sensitivity and acquisition speed [22, 23, and 24]. Entire depth profile (A-scan) is measured from a single spectrum with no mechanical scanning of the reference path. This permits faster acquisition of A-scans using a line scan CCD array and so the use of a fast spectrometer has made video-rate imaging with this technique possible [20,21,22,23]. Acquisition of data at high speed minimizes distortion in the images due to motion of the sample. Also the signal to noise ratio (SNR) of FD-OCT system is

independent of the spectral bandwidth of light source. Thus high resolution imaging is possible with SD-OCT system without any deterioration of SNR [29, 30, 31, 32].

### 1.2 Specific Aim

The primary objective of the research is to design probes for the OCT system and generate high resolution images from it. The images will be then compared with the histological imaging. Also data acquisition hardware will be setup and software will be written for acquiring the data and image processing. To summarize, the specific goals are:

- 1) Setup Michelson interferometer for Fourier domain OCT
- 2) Acquiring and processing the data using Labview and Matlab
- 3) Calibrate and characterize piezoelectric actuator
- 4) Video rate imaging
- 5) Compare the images result with histological imaging
- 6) Make the system more rugged and portable

### 1.3 Organization of the thesis

Chapter 2 describes the background of Fourier domain OCT and piezoelectric actuator as linear scanner. This chapters is divided into three sections where the Fourier domain OCT theory, working principle of piezoelectric actuator and construction of scanning arm using piezoelectric actuator are discussed respectively.

Chapter 3 is an overview of the hardware setup for the Michelson interferometer and OCT probe.

Chapter 4 discussed the calibration and characterization of the OCT system, data acquisition using Labview and image processing using Matlab.

Chapter 5 elaborates the OCT system's performance using both the ex vivo and in vivo probes. Timing issues are also addressed here. It also shows the images taken using both the in vivo and ex vivo probe.

Chapter 6 is a summary of the achievement and limitations the system. It also discussed the future goals and work for improvisation of the system.

CHAPTER 2  
FOURIER DOMAIN OPTICAL COHERENCE TOMOGRAPHY AND  
PIEZOELECTRIC ACTUATOR

2.1 Introduction

Optical techniques are very important for medical imaging fields since they are cost effective, safe and offer higher resolution compare to most of the imaging modalities. Optical coherence tomography[OCT] is a noninvasive imaging technique which was first introduced by Fujimoto et al. [1] in 1991 and it is based on the principles of low coherence interferometry[33] employing Michelson interferometer. Its first applications in medicine were reported less than a decade ago. Specific advantages of OCT are its high axial and lateral resolution, noninvasive and contact free operation. Figure 1 shows the interferometer setup for OCT.

In traditional time domain OCT, broadband low coherence light is used. Light backscattered from the sample is interfered with reflected light from the reference arm. Interference fringes are generated if the optical path lengths of sample and reference arm coincide within the coherence length  $l_c$ . Coherence length  $l_c$  is given by [38]

$$l_c = \frac{2 \ln 2}{\pi} \frac{\lambda^2}{\Delta \lambda} \quad (1)$$

Where  $\lambda_0$  is the mean wavelength, and  $\Delta\lambda$  is the spectral width of the source.

So the reference mirror is rapidly scanned to provide a depth profile (A-Scan) within the sample. Then several A-scans images are stacked together to form a 2 dimensional image (B-Scan) [39, 40].

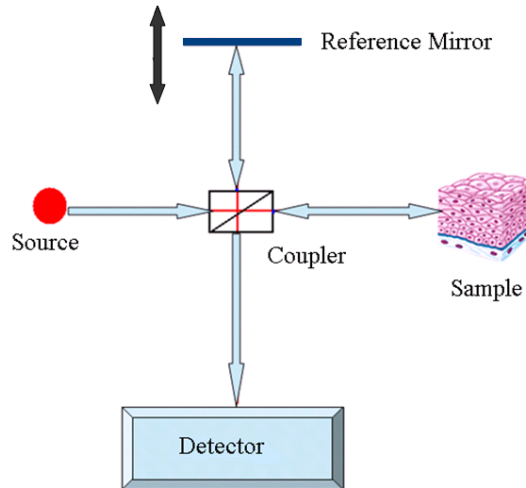


Figure 1: OCT based on low coherence Michelson interferometry

### 2.1.1 Fourier domain Optical Coherence Tomography

We do not need to scan the reference path through depth scan in Fourier domain OCT. Depth information is obtained from the Fourier transformation of the spectrum [42]. A broadband light source is used as the source and the interferometer output is distributed and the spectrum is detected by an array of detectors. The depth profile or A-scan is measured from that spectrum without any mechanical movement of the

reference arm. Video rate imaging has been made possible since it is possible to acquire the data using CCD camera.

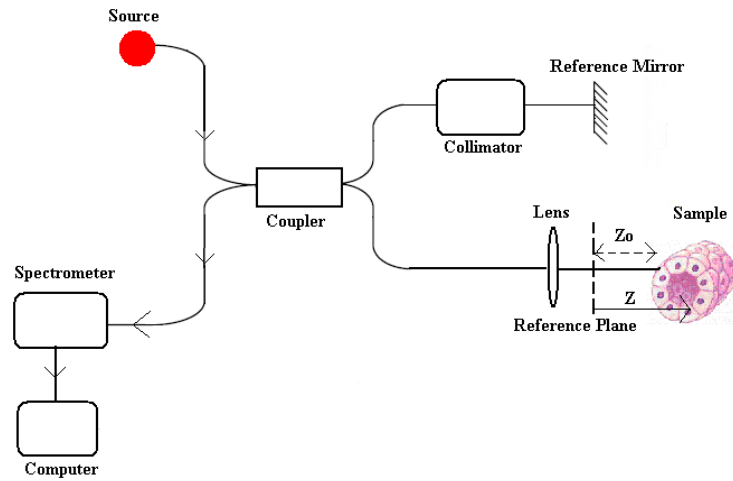


Figure 2: Schematic figure of the FD-OCT system

The interference signal  $I(k)$  is given as [42]:

$$I(k) = S(k) |a_R e^{i2kr} + \int_0^\infty a(z) e^{i2k(r+n(z)-z)} dz|^2 \quad (2)$$

Where,

$r$ : path length in the reference arm

$r + z$  = path length in the object arm

$z_0$  = offset distance between reference plane and object surface

$n$  = refractive index

$a_R$  = amplitude of the reference

$a(z)$  = backscattering amplitude of the object signal



$S(k)$ = spectral intensity distribution of the light source

With some assumption, interference signal  $I(k)$  can be written as:

$$I(k) = S(k) \left| 1 + \int_0^{\infty} a(z) e^{i2knz} dz \right|^2 \quad (3)$$

$$= S(k) \left[ 1 + 2 \int_0^{\infty} a(z) \cos(2knz) dz + \int_0^{\infty} \int_0^{\infty} a(z) a(z') e^{-i2kn(z-z')} dz dz' \right] \quad (4)$$

$a(z)$  can be found by Fourier transformation of  $I(k)$  with the assumption that  $a(z)$  is symmetric with respect to  $z$  i.e.  $a(z) = a(z) + a(-z)$ . We can restrict the equation to  $z > z_0$  which gives the depth information as

$$I(k) = S(k) \left[ 1 + \int_{-\infty}^{\infty} \hat{a}(z) \cos(2knz) dz + \frac{1}{4} \int_{-\infty}^{\infty} \int_{-\infty}^{\infty} \hat{a}(z) \hat{a}(z') e^{-i2kn(z-z')} dz dz' \right] \quad (5)$$

$$I(k) = S(k) \left[ 1 + \int_{-\infty}^{\infty} \hat{a}(z) e^{-i2knz} dz + \frac{1}{4} \int_{-\infty}^{\infty} \int_{-\infty}^{\infty} AC[\hat{a}(z)] e^{-i2knz} dz \right] \quad (6)$$

Where  $AC[\hat{a}(z)]$  is the autocorrelation.

$$I(k) = S(k) \left[ 1 + \frac{1}{2} FOU_z \{ \hat{a}(z) \} + \frac{1}{8} FOU_z \{ AC[\hat{a}(z)] \} \right] \quad (7)$$

Taking the inverse Fourier transform, we get

$$FOU \{ I(k) \} = FOU FOU^{-1} \{ S(k) \} \otimes [(\delta(z))] + \frac{1}{2} \hat{a}(z) + \frac{1}{8} AC(\hat{a}(z)) \quad (8)$$

From this scattering amplitude  $a(z)$  can be found.

### *2.1.2 Application of OCT and optical Biopsy*

Higher resolution and non-invasive has turned OCT into a highly promising technique for biomedical applications. The ultra high resolution imaging capabilities of OCT can provide diagnostic information the microstructure of tissue which cannot be obtained from other imaging modalities. Initially OCT was used for ophthalmic imaging because the available sources could only be used in nearly transparent tissue [33]. Later the imaging depth was increased to around 3 mm which is sufficient for optical biopsy. Conventional biopsy requires excision of tissue specimen which is sometimes unsafe or not possible at all. OCT has the potential to function as ‘optical biopsy’ where morphological information may be assessed using direct, real-time, catheter or endoscopic imaging.[47,48,49] OCT is now useful for performing biopsies, monitoring functional states of human organs, guiding surgical and other treatments and monitoring post-operative recovery processes[49].

## 2.2 Piezoelectric Actuator

### *2.2.1 Background information on Piezoelectric*

It is defined as a physical phenomenon exhibited by certain crystals which change their dimensions when subjected to an Electrical field. This provides a convenient transducer effect between electrical and mechanical oscillations. If an

electrical oscillation is applied to such crystals like ceramic, they will respond with mechanical vibrations.

### 2.2.2 Background information on Stripe actuator

For our OCT probe, we use stripe ceramic actuator of APC International, Ltd. A flexing or bending stripe actuator of APC international is designed to produce a relatively large mechanical deflection in response to an electrical signal. Two thin strips of piezoelectric ceramic are bonded together, usually with the direction of polarization coinciding, and are electrically connected in parallel. When electrical input is applied, one ceramic layer expands and the other contracts, causing the actuator to flex. Parallel electrical configuration ensures high sensitivity to input. Diagram of the internal structure of the stripe actuator was provided to us by APC International Ltd. (Figure 3). Characterization of the stripe actuator for our experiments will be discussed in details in next chapter.

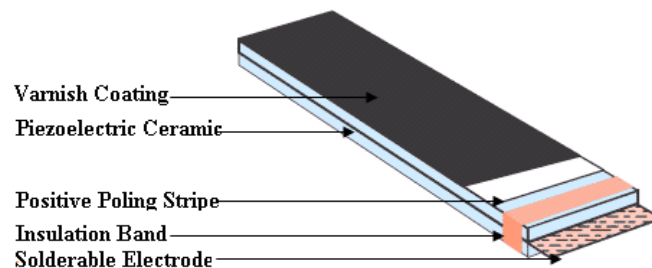


Figure 3: Stripe actuator from APC International Ltd.

### 2.3 Construction of scanning arm (Probe)

The sample path fiber tip was angled cleaved at  $8^{\circ}$ . A glass ferrule was used to house the fiber and a glass tube to house a glass ferrule and the grin lens [Figure 4(a)]. The outer diameter of the glass ferrule is 0.98 mm and the inner diameter of the glass tube is 1 mm. The length and diameter of the grin lens is 2.61 mm and 1.00 mm respectively. The grin lens also has anti-reflection coating. Finally epoxy was used to bond the angle cleaved fiber and the grin lens to the glass tube.

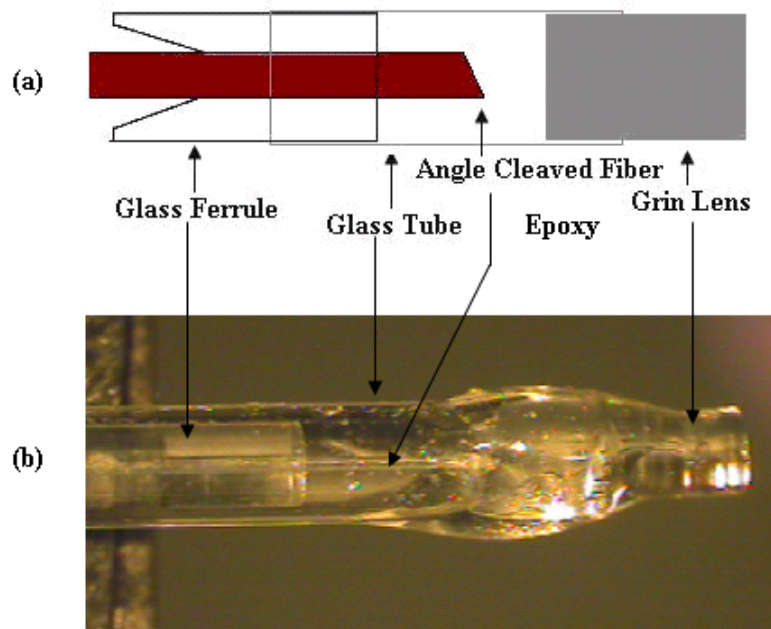
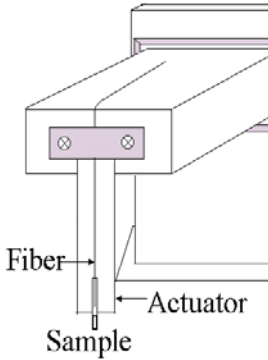
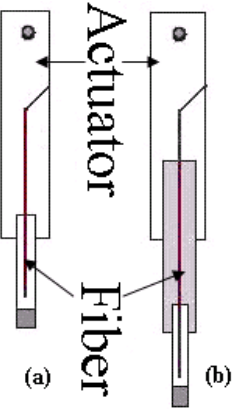
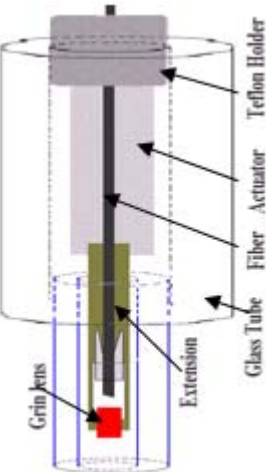


Figure 4: (a) The glass tube housed the glass ferrule where the fiber is placed (b) The actual picture which shows the glass tube, ferrule and the grin lens.

The Grin lens used in the sample path is 1 mm in diameter. The object distance was  $400\mu\text{m}$  and the working distance was 3 mm. The spot size of the beam was found to be  $16\mu\text{m}$  and the corresponding depth of focus was  $420\mu\text{m}$ .

Three different types of probes were designed and tested and these are summarized in Table 1. The resonant frequency of the actuators is 60Hz. During the imaging the resonant frequency has been reduced by adding weight (lead). However, this also reduces the scanning length of the probe.

Table 1: Three different types of probes used

	Probe 1	Probe 2 ( a and b)	Probe 3
Dimension	60 mm x 20 mm	a) 60 mm x 4 mm b) 60 mm x 15 mm	60 mm x 10 mm
Is it covered with a glass tube for protection?	No	No	Yes
schematic diagram	 <p>A schematic diagram of Probe 1. It shows a rectangular actuator block with two circular ports on its top surface. A fiber optic cable is connected to the bottom of the actuator and extends downwards to a small cylindrical sample. Labels include 'Fiber', 'Actuator', and 'Sample'.</p>	 <p>Two schematic diagrams labeled (a) and (b) for Probe 2. Both show a vertical fiber optic cable connected to an actuator block at the top. In (a), the fiber is thin and has a small lead weight at the bottom. In (b), the fiber is thicker and has a larger lead weight at the bottom. Labels include 'Actuator' and 'Fiber'.</p>	 <p>A schematic diagram of Probe 3. It shows a cylindrical glass tube containing a fiber optic probe. The probe has a 'Grin Lens' at the bottom, followed by an 'Extension' section, and a 'Fiber Actuator' section. The entire assembly is held in place by a 'Teflon Holder' at the top. Labels include 'Grin Lens', 'Extension', 'Fiber Actuator', 'Glass Tube', and 'Teflon Holder'.</p>

### *2.3.1 Construction of Probe 1*

The actuator used for Probe 1 has a dimension of 60 mm x 20mm and the resonant frequency is 60 Hz.. OCT imaging using the existing system at the optics lab at UTA requires the scanning frequency should be around 30Hz for the optimum performance. Lower the scanning frequency, higher the number of depth scans we can acquire over a scanning distance and better.

In order to reduce the resonant frequency below than the specified resonant frequency of the actuator, we attached lead (one of the heaviest metal) with the actuator. This will increase the weight and hereby reducing the resonant frequency with a sacrifice of deflection that is lateral scan length will be reduced as well. Sticky tape has been used to attach the optics components (glass tube which house the glass ferrule, grin lens and the fiber) with the actuator.

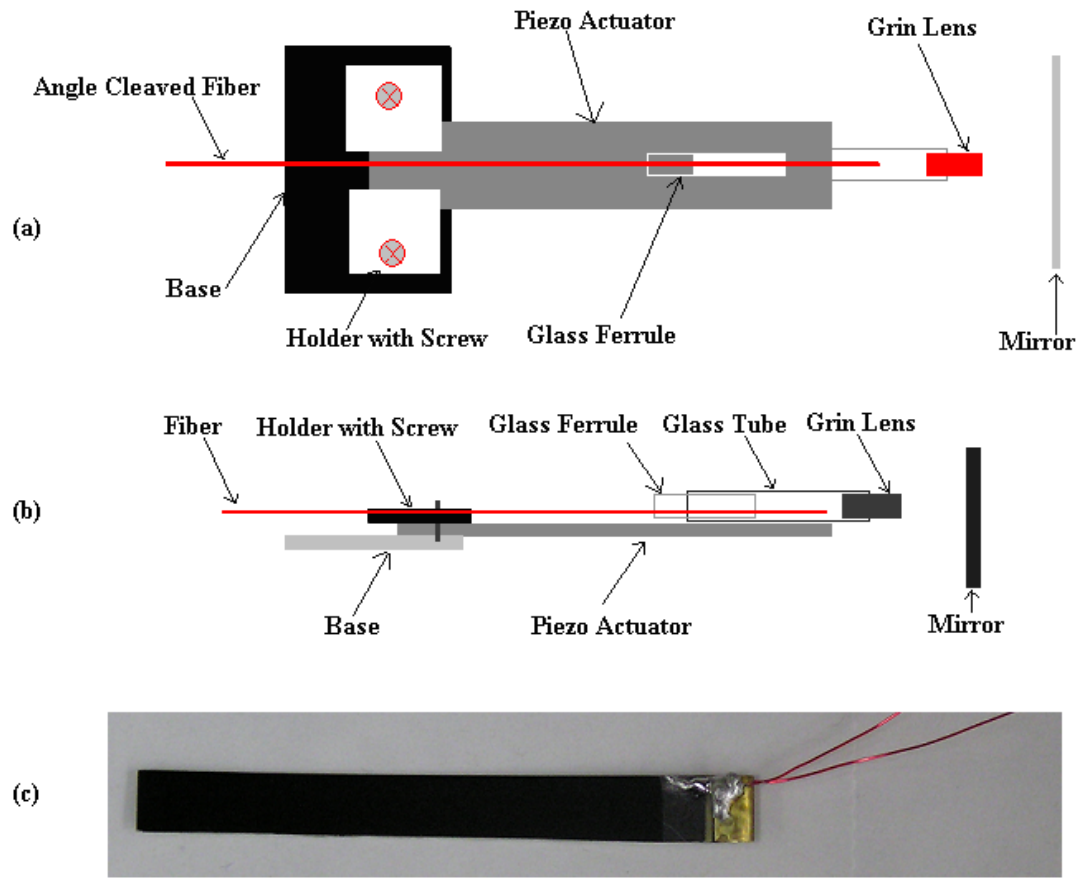


Figure 5: (a) Top view of Probe 1 (b) Side view of Probe 1 (c) Actual Picture of the actuator

### 2.3.2 Construction of Probe 2

The width of the actuator has been reduced using a scissor to construct the probe 2. Two different probes were designed and tested for imaging.

In the first one, an actuator of 60 mm x 4 mm was used. The probe has only 4 mm diameter. Figure 3 shows the actual picture of the probes.

In the second one, a rectangular piezoelectric actuator of 60 mm x 15 mm was used for scanning. An extension of 35 mm length and 2.5 mm diameter was attached with the actuator to increase the free length. Increasing the free length increases the scanning length.

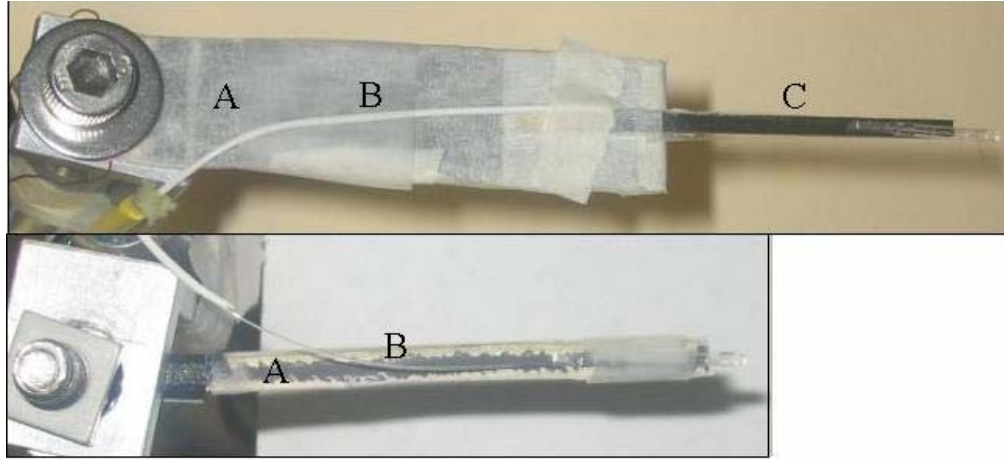


Figure 6: Actual picture of (a) probe2-a and (b) probe2-b

### 2.3.3 Construction of Probe 3

The actuator dimension is 60 mm x 10 mm. Teflon has been used to build a holder for the actuator. Optics components were attached with actuator with a tape. Acrylic tube was used to cover the whole probe. The round Teflon holder's outer diameter is same as the inner diameter of the acrylic tube. Thus the holder along with the actuator stays inside the tube. The inside diameter of the acrylic tube is 6.5 mm which is sufficient for the actuator to vibrate inside the tube.



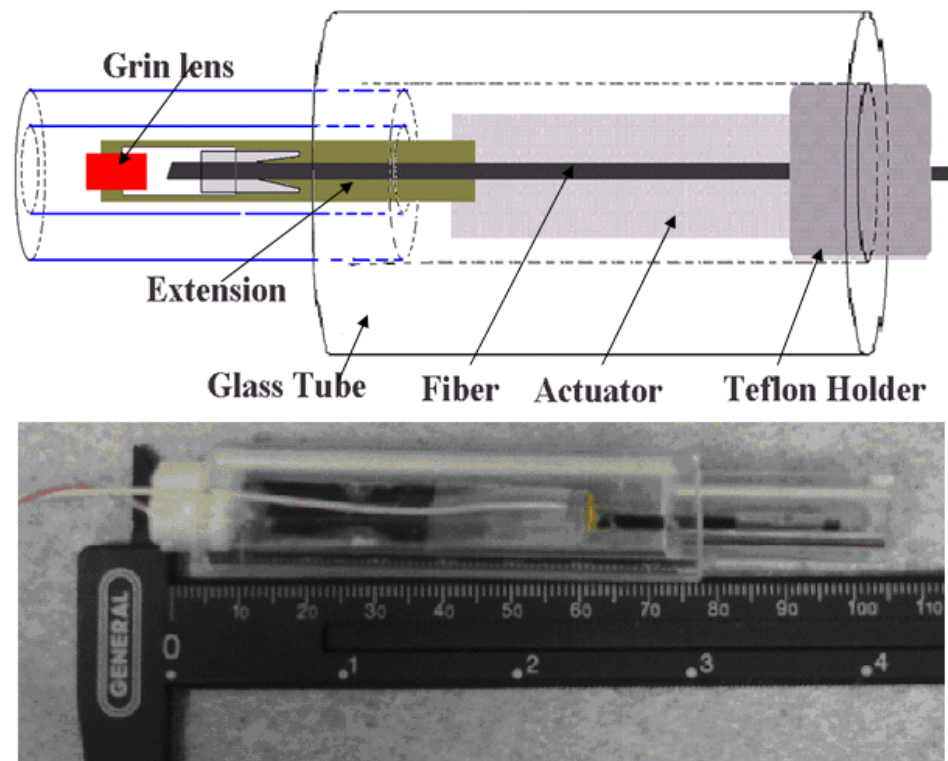


Figure 7: (a) The schematic diagram of the probe (b) The real figure of the probe

CHAPTER 3  
SYSTEM SETUP

3.1 Setup of Michelson Interferometer

The schematic of the OCT system is given in the figure 8.

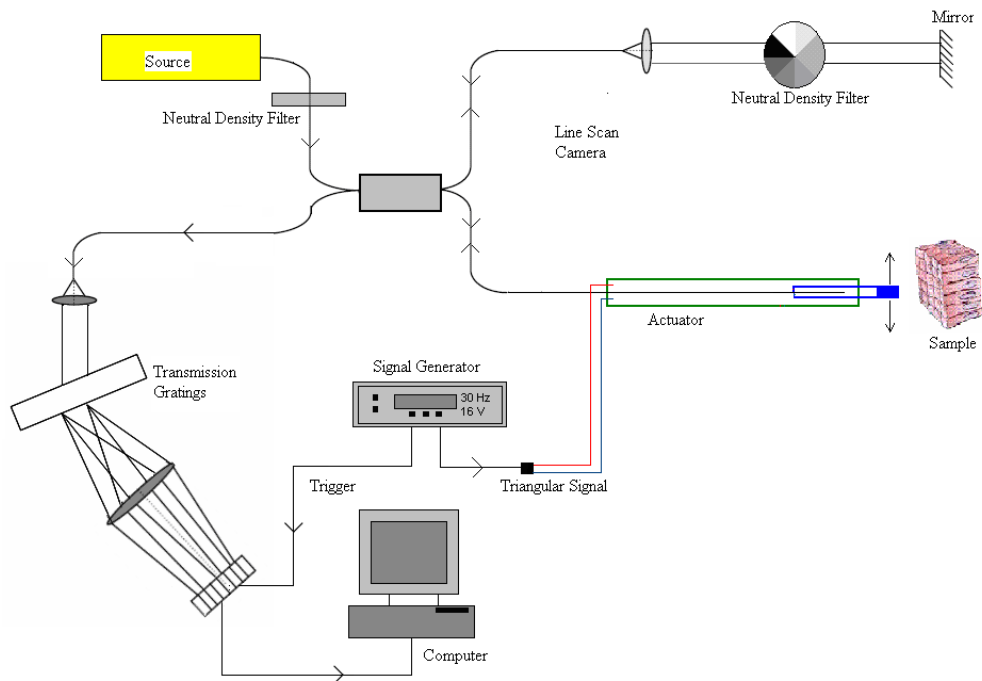


Figure 8: OCT system setup

Figure 8 shows the schematic of the OCT system. Ti-Sapphire broadband laser source capable of lasing in the wavelength range of 700-900 nm was used. The high output power ( $\approx 300$  maw) was attenuated using neutral density filters and coupled into

fiber coupler using a beam coupling assembly. The optical system of the sample arm has a gradient index (GRIN) Lens. The power used for tissue imaging was 9mW. Using a spectrometer the central wavelength was chosen at 830nm with 30 nm FWHM. The signal to noise ratio was found to be 55 dB. Reference arm, with angle cleaved fiber tip, was spliced at one end of the 50/50 coupler. A neutral density filter was used in the reference path to reduce the light reflected back from the reference mirror to match it with that one from the sample tissue.

The light reflected from the sample and the reference mirror was collected at the detector end of the coupler which guides the light through a lens and a diffraction grating to produce a spectrum which contains the depth information. A second lens and a CCD linescan camera were used to collect the spectrum. The CCD linescan camera is mounted on a tip and tilt mount which is mounted on a XYZ translation stage. Tip and tilt mount and the XYZ translation stage is aligned in such a manner so that the CCD array is exactly one focal length away from the focusing lens and fully illuminates the array pixels. The pixels and the corresponding wavelength were calibrated using a commercial spectrometer (ANDO-AQ634) and our CCD array spectrometer.

### 3.2 Probe setup

The working principle is the same for all the probes. The actuator of the probe works as a cantilever and it scans the sample at the resonant frequency. The only difference among those probes is how the actuators are hold as a cantilever.

#### *3.2.1 Probe 1 Setup*

The primary goal of the probe1 is to do tissue imaging. The schematic diagram of the probe1 setup is explained below.

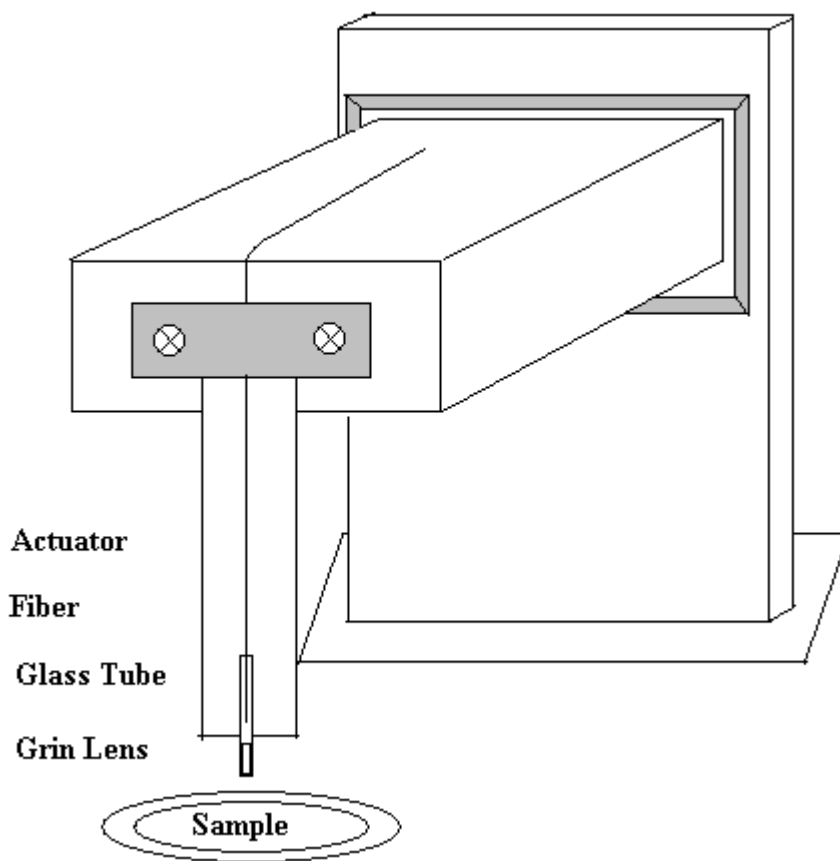


Figure 9: Ex vivo imaging probe setup

and micro stage. The position of the actuator is such that the samples can be kept under the probe. The height of the actuator can be adjusted using the stage. The fiber and the glass tube are kept attached with the actuator using a double stick tape.

### 3.2.2 Probe 2 Setup

The schematic diagram of the probe2 setup is explained below. These probes were connected with the arms of lamps which guided the probe near the tissue sample.

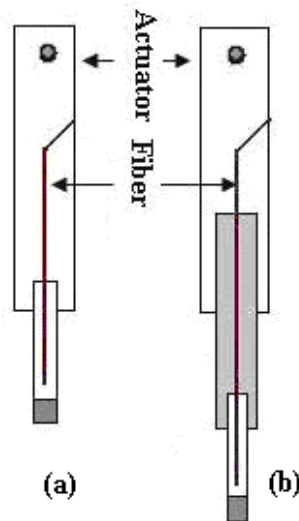


Figure 10: Schematic diagram of Probe2

Here also the actuator is connected with the arm of the lamp with the help of a base plate. The position of the actuator is such that the samples can be kept under the probe. Since the arm of the lamp is flexible, it can be positioned for imaging inside the mouth.

### 3.2.3 Probe 3 Setup

The primary goal of the probe is to do use an acrylic tube for the actuator where the tube can be used for holding. The actuator will be placed inside the tube in such a way that the focus of the light will be at the tip of the tube and so the tube can be placed without the need to keep the sample at focus.

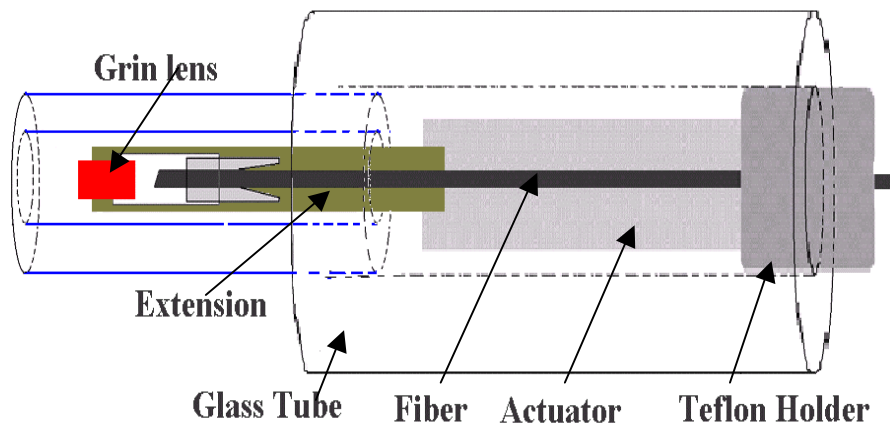


Figure 11: Side View of the probe

CHAPTER 4  
CALIBRATION AND CHARACTERIZATION

4.1 Spectrum Calibration

A commercial spectrometer (ANDO-AQ634) was used to calibrate our CCD line scan camera (ATMEL AVIIVA). There are 2048 pixels in the CCD camera array. Each pixel is 14 micron square with a 12 bit resolution. Wavelength was found from the ANDO-AQ634 spectrometer and corresponding pixel number was found from the camera. Then those value were in Microsoft excel and performed regression analysis.

The relationship was approximated as a 3<sup>rd</sup> order polynomial equation

$$\lambda = m_1 * N + m_2 * N^2 + m_3 * N^3 + \text{Constant} \quad (9)$$

Where  $m_1$ ,  $m_2$ ,  $m_3$  are constant multipliers,  $N$  is the illuminated pixel number and  $\lambda$  is the corresponding wavelength. The R-square value is found to be 0.9989.

The relationship between illuminated pixel  $N$  and corresponding wavelength  $\lambda$  is

$$\lambda = 849.4 - 0.054 * N - 10^{-6} * N^2$$

$$R = 0.9998$$

## 4.2 System characterization

The probes were characterized for the following characteristics

1. Modulation Index
2. Displacement or scan length
3. Resonant Frequency
4. Number of lines per scan
5. Resolution

These characteristics are explained briefly below and are summarized in the table for all the probes used for imaging.

### *4.2.1 Modulation Index*

The modulation index describes by how much the modulated variable of the signal varies around its unmodulated level. The modulation index was calculated by scanning a mirror and by measuring the maximum and minimum value of the detected signal.

$$ModulationIndex = \frac{Amplitude_{(max)} - Amplitude_{(min)}}{Amplitude_{(Average)}}$$

Modulation index varies for all the probes. It depends on the resonant frequency, scan length and the depth of focus.



#### 4.2.2 Scan length

The scan length depends on the deflection of the actuator. The deflection of the actuator depends on the free length and the thickness as given by the equation below:

$$\text{TotalDeflection(mm)} = 2.2 \times 10^{-6} \times \left[ \frac{l_f}{h} \right]^2 V \quad (10)$$

Where,

$l_f$  = free length of actuator

$h$  = thickness of actuator (0.60 mm is standard)

$w$  = width of actuator

$V$  = applied voltage

#### 4.2.3 Resonant Frequency

The resonant frequency of the actuators depends on the free length and the thickness of the actuator.

$$\text{ResonantFrequency(Hz)} = 3.2 \times 10^5 \times \frac{[h]}{[l_f]^2} \quad (11)$$

Again the resonant frequency can also be reduced or dampened by adding weight with the actuators.

#### 4.2.4 Number of lines per scan

Since the number of lines scanned by the camera is fixed (18587lines/second), number of lines that means number of depth scans per second will depends on the scanning frequency of the actuator. The higher the frequency, the lesser lower the number of lines per scan.

#### 4.2.5 Resolution

The resolution will depend upon the coherence length of the source. For a Gaussian spectrum coherence length can be given by

$$l_c = \frac{4 \ln 2}{\pi \lambda_{FWHM}} \lambda_0^2 \quad (12)$$

FWHM implies full width at half maximum of the spectrum. The depth or axial resolution in a FD-OCT system is given as

$$\delta z = \frac{l_c}{2n} = \frac{2 \ln 2}{n \pi \lambda_{FWHM}} \lambda_0^2 \quad (13)$$

where,  $n$  is the refractive index of the medium. Therefore broader spectrum would imply a shorter coherence length and hence give a higher depth resolution.

If  $N$  is the number of pixels that are illuminated by a spectrum of width  $\Delta\lambda$  with the center wavelength at  $\lambda_0$ , the maximum measurable depth,  $\Delta z$  is

$$\Delta z = \frac{\lambda_0^2}{4n\Delta\lambda} N = \frac{\lambda_0^2}{4n\delta\lambda} \quad (14)$$

with  $\delta\lambda$  being the resolution of the spectrometer.

The transverse resolution of OCT system depends on the beam waist  $\Delta x$  on the sample. For a Gaussian beam, the beam waist on the sample is related to the numerical aperture (NA) of the lens and the mean-wavelength  $\lambda$ .

$$\Delta x = \frac{2\lambda}{\pi \cdot NA} = \frac{4\lambda f}{\pi d} \quad (15)$$

where,  $f$  is the focal length of the objective and  $d$  is the beam diameter at the lens. The depth of focus (DOF)  $b$  is given as

$$b = \frac{\pi(\Delta x)^2}{2\lambda} \quad (16)$$

A higher NA lens would provide a higher transverse resolution at the focus at the cost of smaller depth of focus and vice versa. Table 2 summarizes all the parameters for the probes.

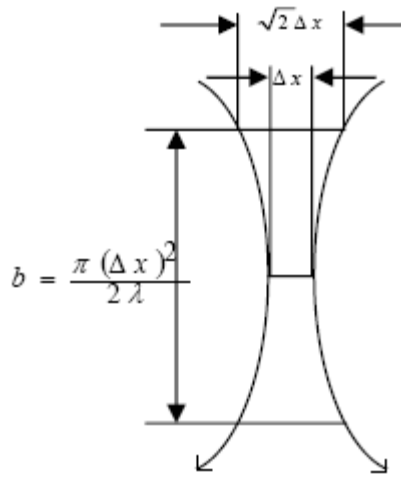
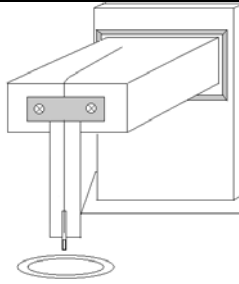
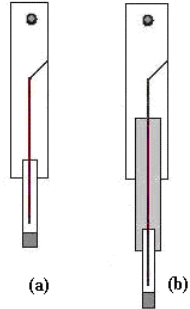
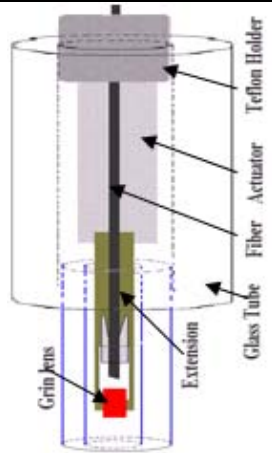


Figure 12: Illustration of depth of focus and the beam waist

Table 2: Characteristics of three different types of probes used

	Probe 1	Probe 2 ( a and b)	Probe 3
schematic diagram			
Modulation Index	64%	(a)64% (b)71%	(c)54%
Effective Scan Length	1.0 mm	(a)0.8 mm (b)1.4 mm	1.0 mm
Number of Lines per scan (Theoretical)	310	(a)265 (b)216	273
Number of Lines per scan(real image)	240	(a)178(b)130	190
Resonant Frequency	30Hz	(a) 35 Hz (b)43 Hz	34Hz
Coherence Length	20 $\mu$ m	20 $\mu$ m	20 $\mu$ m
Axial(depth) Resolution	10 $\mu$ m	10 $\mu$ m	10 $\mu$ m
Lateral Resolution	21 $\mu$ m	21 $\mu$ m	21 $\mu$ m
Depth of Focus	0.5 mm	0.5 mm	0.5 mm

### 4.3 Data Acquisition

Labview was used to view the sample in real time and to acquire the data. Number of samples to be recorded has to be specified in the Labview module before we run the program for data recording. The recorded data were then read by another software module written using Matlab. Matlab read each line recorded by Labview module and then construct one frame from a specified number of lines. Then background was subtracted and the image data was rescaled into k-space. Finally the rolling average was done to reduce the effect of speckle. The flow charts of data acquisition using Labview and data processing using Matlab is given in figure 13 and figure 14 respectively.

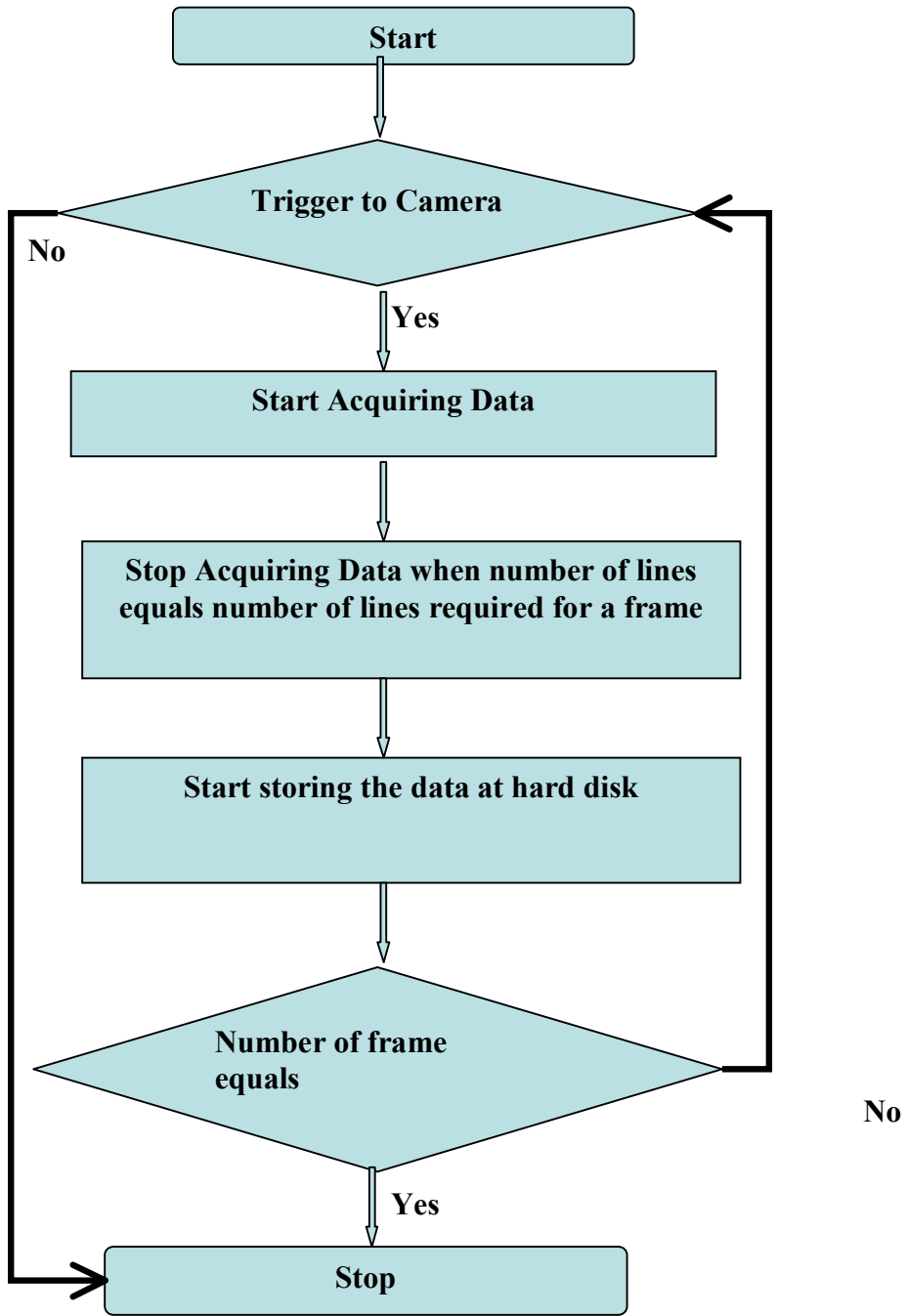


Figure 13: Flowchart for data acquisition using Labview

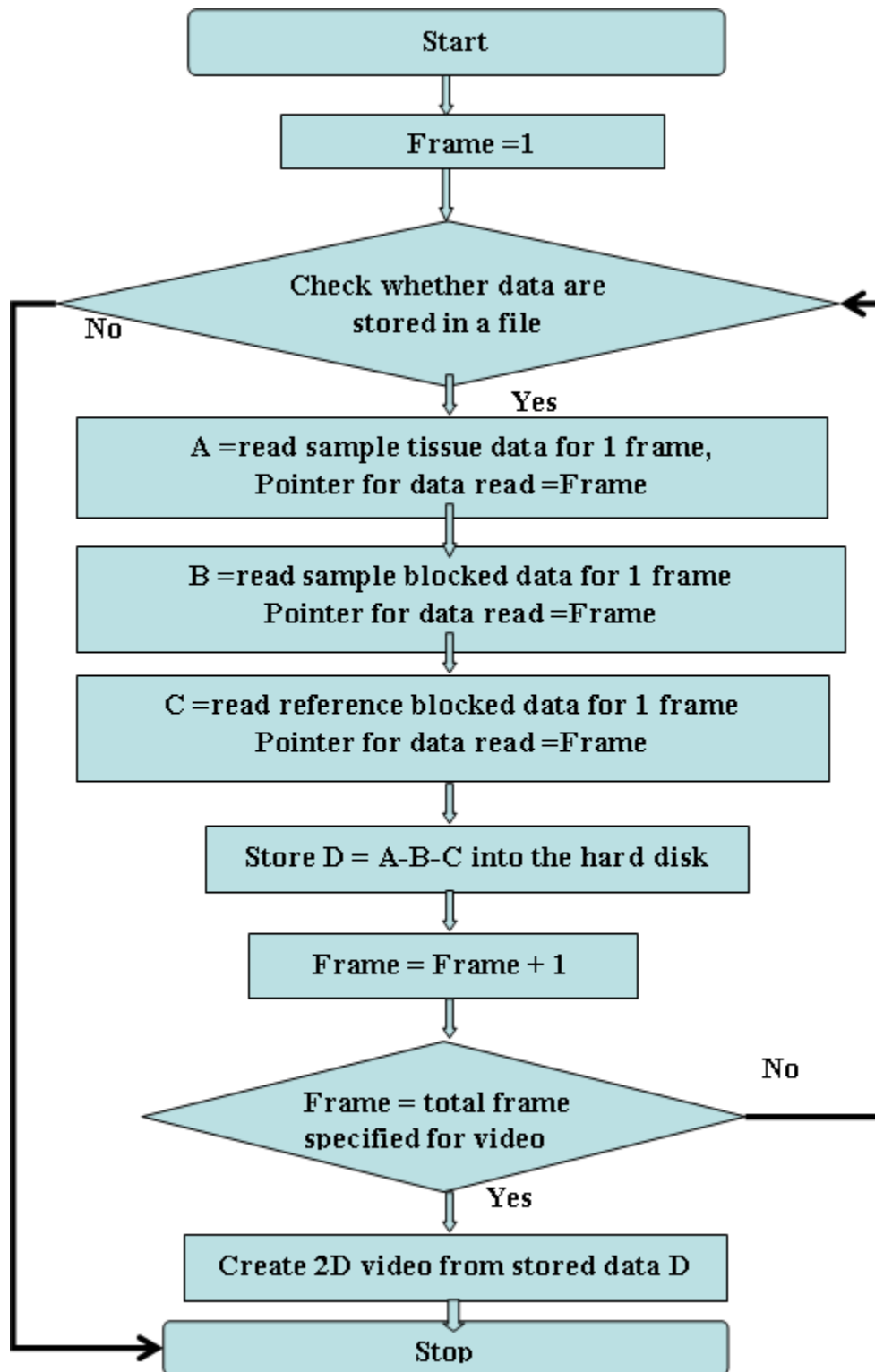


Figure 14: Flowchart for image processing using Matlab

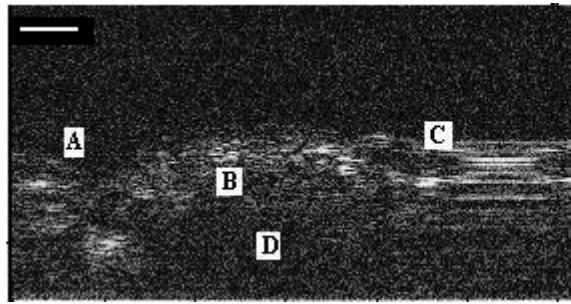
## CHAPTER 5

### RESULTS AND ANALYSIS

#### 5.1 Images Taken By Probe

The probe was fixed on the stage and the sample was positioned below the probe. The images using probe 1 were recorded at 60 frames per seconds with 1.8 mm x 1.0 mm in size (transverse x axial) and each frame consists of 290 A-scans with 1024samples/A-scan. Theoretically number of A-scans per frame should be 310. However, during recording less number of A-scans was reduced to 290 since there was some non-linearity at the edges of the frames. After processing the images, still some non-linear A-scans were found the edges of the frames and those were removed also. Finally the number of A-scans per frames reduced to 240. So the length of the frames presented here has been reduced to 1.4 mm. For each scan, the images of background noises were taken by blocking the sample probe and reference path separately. Then the background subtraction was performed and it was rescaled into k-space and finally the rolling average was done to reduce the effect of speckle. For each scan, the images of background noises were taken by blocking the sample probe and reference path separately. Then the background subtraction was performed and it was rescaled into k-space and finally the rolling average was done to reduce the effect of speckle.





**A: Lumen or Epithelial Layer**  
**B: Lamina Propria**  
**C: Subepithelial Blood Vessel**  
**D: Muscularis**

Figure 15 : OCT image of Normal Urinary bladder 1.4 mm x 0.72 mm. The scale bar represents 120 $\mu$ m.

The finger nail image from probe1 shows nail, eponichium and the cuticles. The image from urinary bladder shows lumen, lamina propria, sub-epithelial blood vessel and muscularis.

## CHAPTER 6

### DISCUSSION AND CONCLUSION

The image shows that in vivo OCT probe has potential to do images of normal as well as cancerous tissues. In the carcinoma the epithelial layer shows dysplasia and the tissue structure does not remain intact. Thus, any changes in epithelial layer, like thickening of the epithelium in to underlying submucosal layer will be evident in OCT images if imaged using the probe.

In summary, in vivo OCT probes have been constructed which are capable of imaging at video rate. One of the biggest advantages of this probe is its low cost. The size of the actuator can be modified without affecting the image quality. So it has the potential to fit inside an instrumentation channel of an endoscope. Currently we are working on designing invivo probe which has ability to distinguish benign and malignant lesions in the early stage of cancer. Currently biopsy and histological examinations are the standard techniques used to detect carcinomas. The OCT images taken with this probe will be compared with gold standard histological images of the same tissue. This optical coherence tomography imaging probe has strong potentials to be able to detect carcinoma of oral mucosa and other in vivo tissues in the early stages and hence can replace the current painful and invasive biopsy technique with non invasive optical biopsy in future.

APPENDIX A

GLOSSARY

Actuator: A device that creates mechanical motion by converting various forms of energy to rotating or linear mechanical energy.

Acrylic: A clear plastic which has moisture barrier as well as waterproofing, water repelling properties.

Endoscope: An instrument used to examine the inside of any part of the body. An illuminated optical instrument that can be inserted through an incision

Ex vivo: Pertaining to a biological process or reaction taking place outside of a living cell or organism

In vivo: Refers to biological processes that take place within a living organism or cell.

Optical Coherence Tomography: An interferometric, non-invasive Optical tomographic imaging technique offering millimeter penetration in tissue with micrometer axial and lateral resolution.

Piezoelectric: A physical phenomenon exhibited by certain crystals which change their dimensions when subjected to an E-field (has an electrical field impressed across it).

Conversely, when subjected to mechanical stress it creates an electrical signal.

Stripe Actuator: Stripe actuators derive their name from a white stripe that denotes the positive surface.

Teflon/ Polytetrafluoroethylene (PTFE): It is a fluoropolymer having the lowest coefficient of friction (against polished steel) of any known solid material. It is also very non-reactive. Appendix A Content

## APPENDIX B

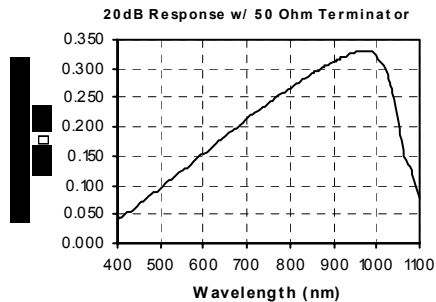
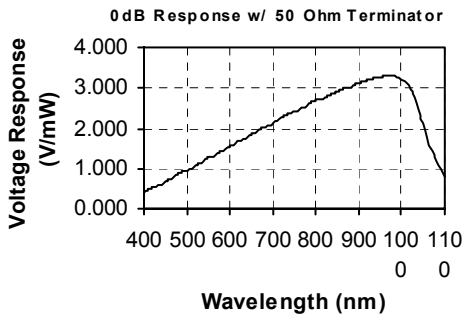
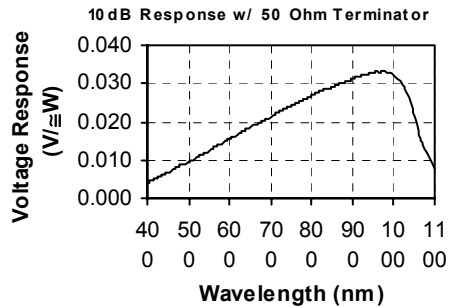
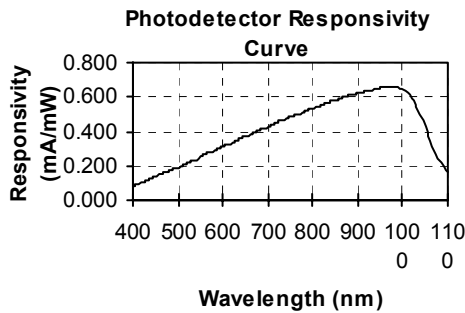
### SPECIFICATION OF THE PHOTO DETECTOR (PDA520)

## PDA520 Operating Manual High Precision Amplified Silicon Detector

**Description:**

The PDA520 is a high precision, high accuracy, low noise, and switchable-gain silicon detector designed for detection of light in the wavelength range of 400 to 1100nm. A three-position rotary switch allows the user to vary the gain in 10 dB steps. A buffered output drives a 50Ω load impedance up to 5 volt. The PDA520 housing includes a removable threaded coupler that is compatible with any number of Thorlabs 1" threaded accessories. This allows convenient mounting of external optics, light filters, apertures, as well as providing an easy mounting mechanism using the Thorlabs cage assembly accessories.

**Graphical Data:**



## APPENDIX C

### BACKGROUND INFORMATION ABOUT STRIPE ACTUATORS

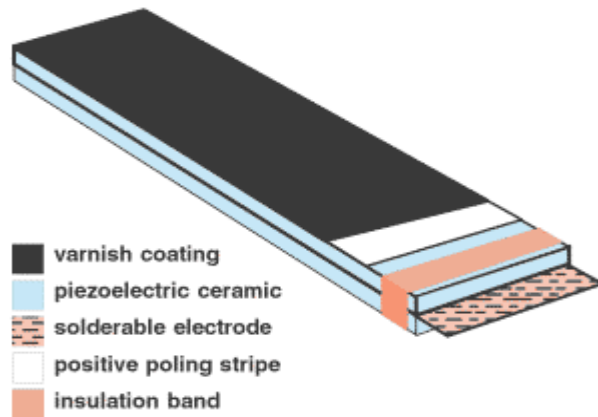
## Stripe™ Actuators

A flexing or bending actuator is designed to produce a relatively large mechanical deflection in response to an electrical signal. Two thin strips of piezoelectric ceramic are bonded together, usually with the direction of polarization coinciding, and are electrically connected in parallel. When electrical input is applied, one ceramic layer expands and the other contracts, causing the actuator to flex. Deflections are large, but blocking forces are low, relative to forces developed by stack actuators. Parallel electrical configuration ensures high sensitivity to input; bias voltage circuitry can prolong the life of the actuator by eliminating the potential for depolarizing the ceramic layers.

### *Stripe Actuator: Better Performance and Longer Lifetime*

- Superior layering technology, for greater range of deflection and useful blocking forces.
- Varnish layer protects surface from humidity and dust.





- Proprietary layering technology increases flexibility, allows greater deflection
- Parallel electrical configuration of ceramic layers ensures high sensitivity to input; compatible with bias voltage circuitry that eliminates the potential for depolarizing the ceramic layers
- Varnish layer electrically insulates surface, protects from humidity, dust, other hazards
- White stripe identifies positive surface
- Solderable electrode bonded between plates
- Thickness tolerance for part without applied coatings

Advanced layering technologies have enabled APC International, Ltd. to develop the Stripe actuator, a flexing actuator that achieves greater deflections than conventional designs. Stripe actuators derive their name from a white stripe that denotes the positive surface.

A standard sized Stripe actuator secured in a cantilever mounting configuration has a deflection range of up to  $>2.5$  mm, in response to a 150 V (maximum) input. If deflection is blocked, a Stripe actuator will develop a useable force. The relationships discussed in technical note [Performance of Stripe Actuators](#) determine the deflections and blocking forces for these actuators.

Vulnerable surfaces of a Stripe actuator are coated with a special varnish that electrically insulates the surface and protects it from humidity, dust, and other hazards

that can shorten the working lifetime of the actuator. A solderable electrode is bonded between the plates.

### Stripe™ Actuators

(Catalog No. 40-)  
Bilaminar, flexing actuators featuring:  
large deflections  
useful blocking forces  
surfaces protected from environmental hazards  
electrical leads / no leads  
custom dimensions available  
competitive pricing  
fast delivery



#### *Typical*

#### *Applications*

Use Stripe actuators in applications that demand sensitivity or a large response:

needle control in textile weaving

Braille machines

accelerometers

opening / closing valves

small-volume pumping devices

switching applications - touch switches - making / breaking electrical contact

cooling devices for electronics (no electromagnetic noise)

## Stripe Actuators

Dimensions (mm)			Free Length (mm)	Total Deflection (mm)	Blocking Force (N)	Resonance Frequency (Hz)	Capacitance (pF)
Long	Wide	Thick					
<i>Catalog No. 40-1010 (600/200/0.60-SA)</i>							
60.0	20.0	0.60	53	>2.5	>0.25	65	170,000
<i>Catalog No. 40-1035 (490/018/0.60-SA)</i>							
49.0	1.8	0.60	42	>1.5	>0.03	110	25,000
<i>Catalog No. 40-1025 (490/021/0.60-SA)</i>							
49.0	2.1	0.60	42	>1.5	>0.05	110	15,000
<i>Catalog No. 40-1040 (400/200/0.60-SA)</i>							
40.0	20.0	0.60	33	>1.0	>0.40	175	115,000
<i>Catalog No. 40-1055 (350/025/0.60-SA)</i>							
35.0	2.5	0.60	28	>0.7	>0.06	245	12,000

Deflections and blocking forces measured at driving voltage of 150 V (maximum) in direction of polarization. Operating temperature: -25°C to 70°C; storage temperature: -40°C to 85°C.

## REFERENCES

- 1) H. D. Huang, E. A. Swanson, C. P. Lin, J. S. Schuman, W. G. Sinson, W. Chang, M. R. Hee, T. Flotte, K. Gregory, C. A. Puliafito, and J. G. Fujimoto, "Optical coherence tomography," *Science* 254, 1178-1181 (1991).
- 2) G. J. Tearney, M. E. Brezinski, B. E. Bouma, S. A. Boppart, C. Pitris, J. F. Southern, J. G. Fujimoto, "In vivo endoscopic optical biopsy with optical coherence tomography," *Science* 276, 2037-2039 (1997).
- 3) J. G. Fujimoto, Mark E. Brezinski, Guillermo J. Tearney, Stephen A. Boppart, Brett Bouma, Michael R. Hee, James F. Southern and Eric A. Swanson, 'Optical biopsy and imaging using optical coherence tomography' *Nature Medicine* 1, 970 - 972 (1995)
- 4) F.I. Feldchtein, V.M. Gelikonov, and G.V. Gelikonov, "Design of OCT Scanners," *Handbook of optical coherence tomography*, B.E. Bouma and G.J. Tearney, Editors, Marcel Dekker, New York(2002).
- 5) P. R. Herz, Y. Chen, A. D. Aguirre, K. Schneider, P. Hsiung, J. G. Fujimoto, K. Madden, J. Schmitt, J. Goodnow, C. Petersen Micromotor endoscope catheter for in vivo, ultrahigh-resolution optical coherence tomography, *Optics Letters*, Vol. 29, Issue 19, pp. 2261-2263 (October 2004)
- 6) Xiumei Liu, Michael J. Cobb, Yuchuan Chen, Michael B. Kimmey, Xingde Li Rapid-scanning forward-imaging miniature endoscope for real-time optical coherence tomography *Optics Letters*, Vol. 29, Issue 15, pp. 1763-1765 (August 2004)
- 7) Yuli Wang, Mark Bachman, Guann-Pyng Li, Shuguang Guo, Brian J. F. Wong, Zhongping Chen Low-voltage polymer-based scanning cantilever for in vivo optical coherence tomography *Optics Letters*, Vol. 30, Issue 1, pp. 53-55 (January 2005)
- 8) Wojtkowski M, Leitgeb R, Kowalczyk A, Bajraszewski T, Fercher AF, "In vivo human retinal imaging by Fourier domain optical coherence tomography," *J Biomed Opt.*, 7(3):457-63. (July 2002).

- 9) S. Yun, G. Tearney, B. Bouma, B. Park, and Johannes de Boer , “High-speed spectral-domain optical coherence tomography at 1.3  $\mu\text{m}$  wavelength”, *Optics Express*, Vol. 11, Issue 26, pp. 3598-3604(December 2004).
- 10) Maciej Wojtkowski, Tomasz Bajraszewski, Piotr Targowski, and Andrzej Kowalczyk, “Real-time in vivo imaging by high-speed spectral optical coherence tomography”, *Optics Letters*, Vol. 28, Issue 19, pp. 1745-1747, (October 2003).
- 11) B. White, M. Pierce, N. Nassif, B. Cense, B. Park, G. Tearney, B. Bouma, T. Chen, and J. de Boer, “In vivo dynamic human retinal blood flow imaging using ultra-high-speed spectral domain optical coherence tomography”, *Optics Express*, Vol. 11, Issue 25, pp. 3490-3497(2003).
- 12) Barry Cense, Nader Nassif, Teresa Chen, Mark Pierce, Seok-Hyun Yun, B. Park, Brett Bouma, Guillermo Tearney, and Johannes de Boer, “Ultrahigh-resolution high-speed retinal imaging using spectral-domain optical coherence tomography” *Optics Express*, Vol. 12, Issue 11, pp. 2435-2447(May 2004).
- 13) Erich Götzinger, Michael Pircher, and Christoph K. Hitzenberger, “High speed spectral domain polarization sensitive optical coherence tomography of the human retina” *Optics Express*, Vol. 13, Issue 25, pp. 10217-10229 (December 2005).
- 14) P H Tomlins and R K Wang “Theory, developments and applications of optical coherence tomography,” *J. Phys. D: Appl. Phys.* 38 No 15, 2519- 2535(7 August 2005).
- 15) Joseph M. Schmitt “Optical Coherence Tomography (OCT): A Review,” *IEEE J. of selected topics in quantum electronics*, 5(4), (July/August 1999).
- 16) M. R. Hee, J. A. Izatt, E. A. Swanson, D. Huang, J. S. Schuman, C. P. Lin, C. A. Puliafito, and J. G. Fujimoto, “Optical coherence tomography for ophthalmic imaging,” *IEEE Engineering in Medicine and Biology*, pp. 67-76(1995).
- 17) G. Häusler, “ Coherence radar and spectral radar -new tools for dermatological diagnosis,” *J. Biomed. Opt.*, 3, 21-31(1998).
- 18) M.W. Lindner, P Andretzky, F Kiesewetter, and A. F. Fercher, “Spectral Radar:Optical Coherence Tomography in the Forier Domain,” *Handbook of Optical Coherence Tomography*, Pages 335-357 (2002).

- 19) R. Leitgeb, W. Drexler, A. Unterhuber, B. Hermann, T. Bajraszewski, T. Le, A. Stingl, and A. Fercher "Ultrahigh resolution Fourier domain optical coherence tomography", *Optics Express*, Vol. 12, Issue 10, pp. 2156-2165(2004).
- 20) F. Fercher, C. K. Hitzenberger, G. Kamp and S. Y. El-Zaiat, "Measurement of intraocular distances by backscattering spectral Interferometry," *ARTICLE Optics Communications*, Volume 117, Issues 1-2, 15 Pages 43-48, (May 1995).
- 21) Yuichi Teramura et al 2000 "Two-dimensional optical coherence tomography using spectral domain interferometry," *J. Opt. A: Pure Appl. Opt.* 2 No 1, Pages 21-26 (January 2000).
- 22) R. A. Leitgeb, C. K. Hitzenberger, and A. F. Fercher, "Performance of Fourier domain vs. time domain optical coherence tomography," *Opt. Express* 11, 889-894 (2003)
- 23) M. A. Choma, M. V. Sarunic, C. Yang, and J. A. Izatt, "Sensitivity advantage of swept source and Fourier domain optical coherence tomography," *Opt. Express* 11, 2183-2189 (2003)
- 24) J. F. de Boer, B. Cense, B. H. Park, M. C. Pierce, G. J. Tearney, and B. E. Bouma, "Improved signal to noise ratio in spectral domain compared with time domain optical coherence tomography," *Opt. Lett.* 28, 2067-2069 (2003).
- 25) N Nassif, B Cense , B H Park, M C Pierce, S H Yun , B E Bouma , G J Tearney, T C Chen and J F de Boer, "In vivo high-resolution video-rate spectral-domain optical coherence tomography of the human retina and optic nerve," *Optics Express*, vol. 12, Issue 3, p.367(2004).
- 26) Rollins, S. Yazdanfar, M. Kulkarni, R. Ung-Arunyawee, and J. Izatt, "In vivo video rate optical coherence tomography," *Opt. Express* 3, 219-229 (1998)
- 27) W. Drexler, U. Morgner, F. X. Krtner, C. Pitris, S. A. Boppart, X. D. Li, E. P. Ippen, and J. G. Fujimoto, "In-vivo ultrahigh-resolution optical coherence tomography," *Optics Letters*, Vol. 24 Issue 17 Page 1221 (September 1999).
- 28) S. H. Yun, G. J. Tearney, B. E. Bouma, B. H. Park, J. F. de Boer, "High-speed spectral-domain optical coherence tomography at 1.3  $\mu\text{m}$  wavelength," *Optics Express*, Vol. 11 Issue 26 Page 3598 (December 2003).
- 29) J. Zhang, J. S. Nelson, and Z. P. Chen, "Removal of a mirror image and enhancement of the signal-to-noise ratio in Fourier-domain optical coherence tomography using an electro-optic phase modulator," *Opt. Lett.* 30, 147 (2005).

- 30) Johannes F. de Boer, Barry Cense, B. Hyle Park, Mark C. Pierce, Guillermo J. Tearney and Brett E. Bouma, "Improved signal-to-noise ratio in spectral-domain compared with time-domain optical coherence tomography," *Optics Letters*, Vol. 28 Issue 21 Page 2067 (November 2003).
- 31) G. Häusler, M.W. Lindner, "Coherence radar and spectral radar – new tools for dermatological diagnosis," *J. Biomed. Opt.* 3, 21-31(1998).
- 32) A.V. Zvyagin, "Fourier-domain optical coherence tomography: optimization of signal-to-noise ratio in full space," *Optics Communications*, Volume 242, Issues 1-3, Pages 97-108(November 2004,).
- 33) H. D. Huang, E. A. Swanson, C. P. Lin, J. S. Schuman, W. G. Sinson, W. Chang, M. R. Hee, T. Flotte, K. Gregory, C. A. Puliafito, and J. G. Fujimoto, "Optical coherence tomography", *Science* 254, 1178-1181, 1991
- 34) Robert C. Youngquist, Sally Carr, and D. E. N. Davies , "Optical coherence-domain reflectometry: a new optical evaluation technique", *Optics Letters*, Vol. 12, Issue 3, pp. 158- 160, 1987
- 35) Fercher AF, Hitzenberger CK, Drexler W, Kamp G, Sattmann H, "In vivo optical coherence tomography", *AM J Ophthalmol* Vol 116, Page 113-4, 1993.
- 36) J. M. Schmitt, A. Knu<sup>ttel</sup>, M. Yadlowsky, and R. F. Bonner, "Optical-coherence tomography of a dense tissue: statistics of attenuation and backscattering," *Phys. Med. Biol.*, vol. 42, pp. 1427-1439, 1994.
- 37) J. M. Schmitt, M. Yadlowsky, and R. F. Bonner, "Subsurface imaging if living skin with optical coherence tomography," *Dermatol.*, vol. 191, pp. 93-98, 1995.
- 38) J. G. Fujimoto, M. E. Brezinski, G. J. Tearney, S. A. Boppart, B. E. Bouma, M. R. Hee, J. F. Southern, and E. A. Swanson, "Optical biopsy and imaging using optical coherence tomography," *Nature Med.*, vol. 1, pp. 970-972, 1995
- 39) F Fercher, W Drexler, C K Hitzenberger and T Lasser "Optical coherence tomography - principles and applications", *Rep. Prog. Phys.* 66 239-303, 2003
- 40) P H Tomlins and R K Wang "Theory, developments and applications coherence tomography," *J. Phys. D: Appl. Phys.* 38 No 15, August 2005
- 41) Joseph M. Schmitt, "Optical Coherence Tomography (OCT): A Review," *IEEE journal of selected topics in Quantum Electronics*, Vol. 5 No 4, August 1999

- 42) Michael A. Bail, Gerd Haeusler, and Juergen M. Herrmann, F. Kieseewetter Michael W. Lindner and A. Schultz, "Optical coherence tomography by spectral radar for the analysis of human skin", *Optical and Imaging Techniques for Biomonitoring III*, Hans-Jochen Foth, Renato Marchesini, Halina Podbielska, Abraham Katzir, Editors, pp. 38-49, January 1998
- 43) N Nassif, B Cense , B H Park, M C Pierce, S H Yun , B E Bouma , G J Tearney, T C Chen and J F de Boer, "In vivo high-resolution video-rate spectral-domain optical coherence tomography of the human retina and optic nerve," *Optics Express*, vol. 12, Issue 3, p.367
- 44) Rollins, S. Yazdanfar, M. Kulkarni, R. Ung-Arunyawee, and J. Izatt, "In vivo video rate optical coherence tomography," *Opt. Express* 3, 219-229 (1998)
- 45) W. Drexler, U. Morgner, F. X. Krtner, C. Pitris, S. A. Boppart, X. D. Li, E. P. Ippen, and J. G. Fujimoto, "In-vivo ultrahigh-resolution optical coherence tomography," *Optics Letters*, Vol. 24 Issue 17 Page 1221 (September 1999)
- 46) S. H. Yun, G. J. Tearney, B. E. Bouma, B. H. Park, J. F. de Boer, "High-speed spectral-domain optical coherence tomography at 1.3  $\mu\text{m}$  wavelength," *Optics Express*, Vol. 11 Issue 26 Page 3598 (December 2003)
- 47) Andrew M. Rollins, Rujchai Ung-arunyawee, Amitabh Chak, C. K. Wong, Kenji Kobayashi, Michael V. Sivak Jr. and Joseph A. Izatt, "Real-time in vivo imaging of human gastrointestinal ultrastructure by use of endoscopic optical coherence tomography with a novel efficient interferometer design," *Optics Letters*, Vol. 24, Issue 19, pp. 1358-1360 (October 1999)
- 48) F. Feldchtein, G. Gelikonov, V. Gelikonov, R. Kuranov, A. Sergeev, N. Gladkova, A. Shakhov, N. Shakhova, L. Snopova, A. Terent'eva, E. Zagainova, Y. Chumakov, and I. Kuznetzova, "Endoscopic applications of optical coherence tomography," *Opt. Express* 3, 257-270 (1998).
- 49) P. R. Herz, Y. Chen, A. D. Aguirre, K. Schneider, P. Hsiung, J. G. Fujimoto, K. Madden, J. Schmitt, J. Goodnow, and C. Petersen, "Micromotor endoscope catheter for in vivo, ultrahigh-resolution optical coherence tomography," *Opt. Lett.* 29, 2261-2263 (2004).



## BIOGRAPHICAL INFORMATION

Asif Rizwan was born on March 15, 1980 in Dhaka, Bangladesh. He completed his schooling from Jahangirnagar University School and College, Bangladesh and received his Bachelor's degree in Electrical and Electronics Engineering from Bangladesh University of Engineering and Technology, Bangladesh in 2004. He served as Lecturer in the department of 'Electronics and Telecommunication Engineering' at Daffodil International University, Bangladesh for about six months.

In Fall, 2004 he started his graduate studies in Joint Program of Biomedical Engineering at the University of Texas at Arlington and University of Texas Southwestern Medical Center at Dallas. He joined the biomedical optics lab as a Graduate Research Assistant and implemented a miniature Optical Coherence Tomography probe.